Theoretical simulation and experimental validation of inverse quasi-one-dimensional steady and unsteady glottal flow models

Julien Cisonni,[a] Annemie Van Hirtum, and Xavier Pelorson
Department of Speech and Cognition, GIPSA-Laboratory, UMR CNRS 5216, Grenoble Universities, 961 rue de la Houille Blanche, BP 46, 38402 Saint Martin d'Heres, France

Jan Willems
Department of Applied Phusics, Gas Dynamic and Aero-acoustics, Eindhoven University of Technology, P.O. Box 513, CC 2.24, 5600 MB, Eindhoven, The Netherlands

(Received 30 October 2007; revised 23 April 2008; accepted 23 April 2008)

In physical modeling of phonation, the pressure drop along the glottal constriction is classically assessed with the glottal geometry and the subglottal pressure as known input parameters. Application of physical modeling to study phonation abnormalities and pathologies requires input parameters related to *in vivo* measurable quantities commonly corresponding to the physical model output parameters. Therefore, the current research presents the inversion of some popular simplified flow models in order to estimate the subglottal pressure, the glottal constriction area, or the separation coefficient inherent to the simplified flow modeling for steady and unsteady flow conditions. The inverse models are firstly validated against direct simulations and secondly against *in vitro* measurements performed for different configurations of rigid vocal fold replicas mounted in a suitable experimental setup. The influence of the pressure corrections related to viscosity and flow unsteadiness on the flow modeling is quantified. The inversion of one-dimensional glottal flow models including the major viscous effects can predict the main flow quantities with respect to the *in vitro* measurements. However, the inverse model accuracy is strongly dependent on the pertinence of the direct flow modeling. The choice of the separation coefficient is preponderant to obtain pressure predictions relevant to the experimental data.
 [DOI: 10.1121/1.2931959]

PACS number(s): 43.70.Bk, 43.70.Jt [BHS] Pages: 535–545

I. INTRODUCTION

Physical modeling of phonation or voiced sound production intends to predict the vocal folds oscillatory behavior in terms of relevant physical and physiological quantities. Physical modeling is, in particular, interesting for the study of irregular phonation patterns or vocal folds dysfunction due to pathology (Kreiman and Gerratt, 2005; Mergell *et al.*, 2000; Wong *et al.*, 1991; Wurzbacher *et al.*, 2006; Zhang and Jiang, 2004). Despite the development of clinical *in vivo* measurement techniques, the observation and quantification of phonation in either normal or disordered conditions remains a difficult task often depending on invasive or indirect measurement methods (Cranen and Boves, 1988; Hertegard and Gauffin, 1995; Qiu and Schutte, 2006; Sundberg *et al.*, 1999; Svec *et al.*, 2007). Consequently, the subglottal pressure and the glottal aperture, which are the main input parameters for standard physical phonation models, are difficult to be obtained directly from *in vivo* measurements. The influence of the input parameter set on the model outcome is often assessed following an analysis-by-synthesis approach and is further compared to *in vivo* measured quantities (Drioli, 2005; Sciamarella and d'Alessandro, 2004; Wurzbacher *et al.*, 2006). Therefore, the interest of inverting classical physical phonation models is multiple and could, besides a purely scientific interest, lead to the development of noninvasive measurement techniques. At long term, inverse physical models might be validated on *in vivo* data and eventually be applied in pathological conditions or in favor of advanced voice synthesis. Moreover, in a clinical context, inverse models allow one to account for subject-dependent data. Most of the studies considering inversion of phonation models deal with inverse filtering techniques in order to estimate the glottal volume flow rate from which quantitative parameters describing the glottal source can be derived (Alku *et al.*, 1998; Frohlich *et al.*, 2001; Pelorson, 2001; Price, 1989; Rothenberg and Zahorian, 1977; Shadle *et al.*, 1999). Although inverse filtering is successful for phonation quantification purposes, it is limited to a parametrized voice source description in terms of the estimated volume flow rate. Since inverse filtering does not rely on a physical flow model and often adopts the source-filter model (Fant, 1960) neglecting glottal-supraglottal interaction, it is unable to account for the fluid-structure interaction between the vocal fold tissue and the glottal airflow during phonation. Inverting physical phonation models is interesting to obtain biomechanical data and flow properties relevant to the phonation mechanism. A first attempt to tune the parameters of a physical low dimensional glottal model to the volume flow rate obtained from inverse filtering following an analysis-by-

[a]Electronic mail: julien.cisonni@gipsa-lab.inpg.fr

synthesis approach is presented in Drioli (2005). Considering the inversion of biomechanical models, an encouraging result is presented for arteries where tissue characteristics are deduced from blood flow measurements (Lagrée, 2000). The current research explores the inversion of simplified quasi-one-dimensional flow models widely applied in classical direct phonation models (Lous *et al.*, 1998; Pelorson *et al.*, 1994; Ruty *et al.*, 2007). The aimed models are derived from Bernoulli's one-dimensional flow equation corrected for viscous effects and flow unsteadiness. The use of simplified flow theories in order to estimate the important phonation quantities, as phonation onset threshold pressure and oscillation frequency, obtained in an *in vitro* context is discussed in Ruty *et al.* (2007) and Van Hirtum *et al.* (2007). At first, direct flow models are outlined and inverse models are formulated. Then, theoretical simulations are presented in order to validate the inverse flow model outcome against the direct model input. Next, inverse flow models are validated on experimental *in vitro* data obtained with rigid glottal replicas for different glottal constriction shapes and flow conditions. The inverse modeling performance is discussed with respect to the accuracy of the direct modeling.

II. DIRECT AND INVERSE FLOW MODELS

Low-order physical phonation models exploit simplified flow models to describe the glottal airflow and the resulting pressure forces exerted on the vocal fold tissue. The underlying assumptions necessary to use simplified flow models are briefly outlined in Sec. II A. Next, direct simplified flow models are formulated in Sec. II B and inverse flow models are described in Sec. II C.

A. Assumptions and nondimensional numbers

The flow models described in Ruty *et al.* (2007) account for severe assumptions on the flow behavior through the glottal constriction. The assumptions are motivated by a nondimensional analysis of the governing *Navier–Stokes* equations while accounting for typical values of physiological geometrical and flow characteristics in case of normal phonation by a male adult (Deverge *et al.*, 2003; Pelorson *et al.*, 1994; Ruty *et al.*, 2007; Vilain *et al.*, 2004). The main nondimensional numbers considered are the geometrical aspect ratio $r_{l_g}=h_g/l_g$, *Mach* number $M=v/c_0$, *Reynolds* number $\mathrm{Re}=vh/\nu$, and *Strouhal* number $\mathrm{Sr}=fL/v$, where h_g denotes the minimum aperture, l_g is a typical width normal to the flow direction and to the constriction, v is a characteristic flow velocity, $c_0=350$ m/s is the speed of sound, h is a typical dimension, $\nu=1.5\times10^{-5}$ m^2/s is the kinematic air viscosity, L is the constriction length in the flow direction, and f is a characteristic frequency. Typical physiological values for glottal flow during voice production yields the following order of magnitudes for the nondimensional numbers: $r_{l_g}\sim O(10^{-1})$, $M^2\sim O(10^{-4})$, $\mathrm{Re}=v_g h_g/\nu\sim O(10^3)$, $\mathrm{Sr}\sim O(10^{-2})$ with v_g as the flow velocity at the minimum aperture. These typical values allow one to assume the flow as one dimensional, incompressible, laminar and quasisteady. The glottal area, $A(x)=l_g h(x)$, normal to the flow direction x, is assumed to be rectangular with fixed width l_g and glottal height $h(x)$ which only varies along the flow direction, as shown in Fig. 1. Although viscous effects can be negligible for the main flow, viscosity is expected to be important near the walls and the resulting effects are discussed in Sec. II B 1.

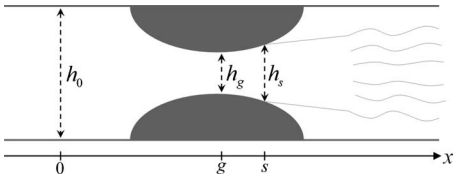

FIG. 1. Schematic representation of the glottal geometry. The x dimension indicates the flow direction. 0, g, and s indicate the positions of the origin, minimum aperture, and flow separation along the channel. The corresponding heights are indicated.

B. Direct simplified flow models

1. Direct flow models description

Under the assumptions of one-dimensional, laminar, fully inviscid, steady and incompressible flow, the one-dimensional *Bernoulli's equation* can be used to estimate the pressure distribution along the glottal constriction, where $\rho=1.2$ kg/m^3 indicates the mean air density. Therefore, the pressure difference $\Delta P_B(a,b,t)=p_a(t)-p_b(t)$ between two positions, a and b, along the constriction in the x dimension yields with $a<b$

$$\Delta P_B(a,b,t)=\frac{1}{2}\rho\frac{\Phi^2}{l_g^2}\left(\frac{1}{h_b(t)^2}-\frac{1}{h_a(t)^2}\right) \tag{1}$$

for a rectangular glottal geometry with area $A(x,t)=l_g h(x,t)$. The quantities $h_a(t)$ and $h_b(t)$ correspond to the constriction heights at positions a and b in the flow direction, while $\Phi(t)=v(x,t)A(x,t)=v(x,t)h(x,t)l_g=\mathrm{const}$ denotes the volume flow rate which is assumed to be constant along the constriction.

In order to predict a pressure drop across the constriction and hence to be useful, Eq. (1) needs to be corrected to account for the flow separation and jet formation in the diverging part of the constriction downstream of the minimum aperture $h_g(t)$ (Pelorson *et al.*, 1994). The turbulent jet formation downstream of the separation point is due to very strong viscous pressure losses and thus cannot be predicted by the Bernoulli law (Alipour and Scherer, 2006; Grandchamp *et al.*, 2007). In literature, the area associated with flow separation $A_s(t)$ is empirically *ad hoc* chosen as 1.1, 1.2, or 1.3 times the minimum glottal constriction area $A_g(t)$, i.e., $A_s(t)=c_s A_g(t)$ with $c_s=A_s(t)/A_g(t)\geqslant 1$ the *ad hoc* separation coefficient (Deverge *et al.*, 2003; Hofmans *et al.*, 2003; Lucero, 1999; Pelorson *et al.*, 1994). Accounting for a rectangular glottal area, the separation criterion becomes $c_s=h_s(t)/h_g(t)\geqslant 1$. The separation position and corresponding height $h_s(t)$ are indicated with s and $h_s(t)$, respectively, in Fig. 1. Consequently, Eq. (1) only holds down to the separation point and, therefore, c_s is an important parameter in the flow model. The pressure in the constriction after the separation point is considered to be equal to the downstream pressure. In addition to the occurrence of flow separation, the

preceding assumption of inviscid flow is also not valid for low Reynolds numbers. This is the case for small constriction heights where viscous effects cannot be neglected (Blevins, 1992; Kundu, 1990). To account for the pressure drop induced by viscous friction along the walls, an additional *Poiseuille* term $\Delta P_P(a,b,t)$ can be added to the Bernoulli term (1)

$$\Delta P_P(a,b,t) = 12\mu \frac{\Phi}{l_g} \int_a^b \frac{dx}{h(x)^3}, \tag{2}$$

where μ is the dynamic viscosity of the fluid and again $a < b$. The *Poiseuille* term $\Delta P_P(a,b,t)$ assumes a nonuniform parabolic two-dimensional velocity profile and therefore presents a viscosity related correction to the one-dimensionality assumed in Eq. (1). Although several *in vitro* experimental studies confirm the quasisteady approximation made in Eq. (1) (Deverge *et al.*, 2003; Hofmans *et al.*, 2003; Vilain *et al.*, 2004; Zhang *et al.*, 2002), pressure differences induced by flow unsteadiness due to the fluctuations of $h(x,t)$, related to wall movements and/or $p_0(t)$ in time, are important for high frequency variations and/or vocal folds wall vibrations involving collision or glottal closure (Deverge *et al.*, 2003; Vilain *et al.*, 2004). The additional pressure loss $\Delta P_U(a,b,t)$ due to the resulting unsteadiness in the volume airflow $\Phi(t)$ is expressed as

$$\Delta P_U(a,b,t) = \frac{\rho}{l_g} \int_a^b \frac{d}{dt}\left(\frac{\Phi(t)}{h(x,t)}\right) dx. \tag{3}$$

2. Direct flow models, input and output

From the pressure terms outlined in Sec. II B 1, several classical direct flow models can be considered. The physical variables defining their input and output, and the inherent model parameters are pointed out. For all direct flow models, the pressure upstream of the constriction is the main driving control parameter. This pressure is labeled $p_0(t)$ in correspondence with the 0 position indicated in Fig. 1. The downstream pressure at flow separation and beyond is assumed to be equal to the atmospheric pressure p_{atm} which corresponds to zero since all pressures are expressed relatively to p_{atm}, i.e., $p_s(t)=0$ Pa. The flow separation position $x=s$ is determined by the value of the separation coefficient c_s. Since the flow separation position determines the flow model outcome to a large extent, the coefficient c_s is an important inherent model parameter. Other known inherent model parameters are the required physical constants μ, ρ, and the glottal width l_g. The constriction geometry, which is characterized by the channel height $h(x,t)$ illustrated in Fig. 1, is assumed to be known. The pressure distribution along the constriction, i.e., $p(x,t)$ with $0 \leqslant x \leqslant s$, is estimated from the pressure difference $\Delta P(0,x,t)=p_0(t)-p(x,t)$ which can be defined by the addition of the pressure terms (1)–(3). Thus, four direct flow models based on the pressure term combinations presented in Table I are under consideration: steady Bernoulli model (BS-d), steady Poiseuille model (PS-d), unsteady Bernoulli model (BU-d), and unsteady Poiseuille model (PU-d).

For each of the four flow models, the input parameters are the set $(p_0(t),h(x,t),c_s(t))$, where $p_0(t)$ and $h(x,t)$ characterize the physical problem and $c_s(t)$ is a parameter inherent to the chosen modeling approach. The direct flow model output $(p(x,t),\Phi(t))$ is obtained in two steps. First, the volume flow rate $\Phi(t)$ is estimated from the total pressure difference across the constriction $\Delta P(0,s,t)$. Next, the pressure profile $p(x,t)$ along the constriction is obtained from the upstream pressure $p_0(t)$ and the retrieved $\Phi(t)$ value.

TABLE I. Pressure terms used in the four direct flow models.

Flow model	ΔP_B	ΔP_P	ΔP_U
BS-d	x		
PS-d	x	x	
BU-d	x		x
PU-d	x	x	x

C. Inverse simplified flow models

In this section, inverse flow models derived from each of the four direct flow models detailed in Sec. II B 2 are formulated. The assumptions discussed in Secs. II A and II B 1 extend naturally to the proposed inverse models. Therefore, the estimation of the physical quantities obtained with the proposed inverse flow models are *a priori* subjected to the same limitations as their direct counterparts. Further approximations might be introduced due to the applied inversion strategies outlined in Sec. II C 2. The inverse model variables and parameters are discussed in the following section.

1. Inverse flow models, input and output

The pressure distribution $p(x,t)$ is the main output quantity of the direct flow models. In the presented inverse flow models, the role of direct flow model input and output variables are interchanged. The pressure at the minimum constriction height $p_g(t)$ is therefore considered as the known input quantity of the inverse models. From the direct flow models previously described, three different cases of inverse problems are defined. Firstly, the upstream pressure $p_0(t)$ is the unknown quantity (inverse model 1). Secondly, the minimum constriction height $h_g(t)$ is searched (inverse model 2). Thirdly, the flow separation coefficient c_s is estimated (inverse model 3). Each of the four direct models outlined in Sec. II B 2 can be exploited to resolve the three inversion problems in order to retrieve the quantities of interest, as shown in Table II.

The interest of the first inversion problem, i.e., to retrieve the upstream pressure $p_0(t)$, is obvious since it is the main driving parameter of the direct phonation flow models determining the total pressure difference across the glottal

TABLE II. Input and output variables of the three inverse problems.

	Input	Output
Direct model (-d)	$p_0(t)$, $h_g(t)$, $c_s(t)$	$p_g(t)$, $\Phi(t)$
Inverse problem 1 (-inv1)	$p_g(t)$, $h_g(t)$, $c_s(t)$	$p_0(t)$, $\Phi(t)$
Inverse problem 2 (-inv2)	$p_0(t)$, $p_g(t)$, $c_s(t)$	$h_g(t)$, $\Phi(t)$
Inverse problem 3 (-inv3)	$p_0(t)$, $h_g(t)$, $p_g(t)$	$c_s(t)$, $\Phi(t)$

constriction. In human phonation p_0 corresponds to the subglottal pressure which is, as outlined in the introduction, very hard to retrieve from *in vivo* measurements. The glottal constriction geometry $h(x,t)$ is also a main known input parameter in direct flow modeling. Assuming a known geometrical shape for the constriction, the geometry is fully characterized by the minimum constriction height $h_g(t)$. Therefore, the second inversion problem consists in estimating $h_g(t)$. Although c_s is not a physical quantity, this parameter allows to account for major physical phenomena, i.e., flow separation and jet formation. Since the value of c_s acts to a large extent on the accuracy of the direct flow models, it is quite an issue in the literature (Alipour and Scherer, 2004; Deverge *et al.*, 2003; Hofmans *et al.*, 2003; Lucero, 1999; Pelorson *et al.*, 1994) and the third inverse problem consists in estimating this parameter. The resulting inverse models and the related inversion strategies are discussed in the next section.

2. Inverse flow models description and inversion strategies

The applied inversion strategies are adapted with respect to the direct quasi-one-dimensional flow model under consideration. In the following, the quantities estimated by the models are designated by $\hat{p}_g(t)$, $\hat{p}_0(t)$, $\hat{h}_g(t)$, $\hat{c}_s(t)$, and $\hat{\Phi}(t)$.

a. Inverse steady Bernoulli model. Inversion of the steady Bernoulli model (BS-d) given by Eq. (1) is easily obtained analytically. Firstly, the upstream pressure $\hat{p}_0(t)$ is retrieved as

$$\hat{p}_0(p_g(t),h(x,t),c_s(t),t) = p_g(t)\frac{c_s^2(t)h_g^2(t) - h_0^2}{h_0^2(c_s^2(t)-1)}. \quad (4)$$

Secondly, the minimum constriction height $\hat{h}_g(t)$ becomes

$$\hat{h}_g(p_g(t),p_0(t),c_s(t),t) = \frac{h_0}{c_s(t)}\sqrt{1+\frac{p_0(t)}{p_g(t)}(c_s^2(t)-1)}. \quad (5)$$

Thirdly, the separation coefficient $\hat{c}_s \geqslant 1$ is given as

$$\hat{c}_s(p_g(t),p_0(t),h_g(t)) = h_0\sqrt{\frac{p_0(t)-p_g(t)}{p_0(t)h_0^2 - p_g(t)h_g^2(t)}}. \quad (6)$$

Applying the assumption $h_0 \gg h_g$, the expression for $\hat{c}_s$ simplifies to

$$\hat{c}_s(t) \approx \sqrt{1-\frac{p_g(t)}{p_0(t)}} \Rightarrow \frac{p_g(t)}{p_0(t)} \approx 1-\hat{c}_s^2(t), \quad (7)$$

which illustrates that the parameter c_s determines the importance of the pressure drop at the minimum constriction height relatively to the upstream pressure p_0. Equation (7) also indicates that the steady Bernoulli model can only predict $\hat{p}_g \leqslant 0$ since $p_0 \geqslant 0$ and $c_s \geqslant 1$.

b. Inverse steady Poiseuille model. Inversion of the steady Poiseuille model (PS-d) defined by the sum of pressure terms (1) and (2) can not be achieved analytically. Therefore, a numerical iterative method is applied in order to invert the model (Kelley, 1995). This way, each of the three inversion problems becomes a classical minimization problem. By considering $\hat{p}_g(t)$ as a function of $p_0(t)$, $h_g(t)$, and $c_s(t)$, i.e., $\hat{p}_g(t)=f(p_0(t),h_g(t),c_s(t))$, the three inversion problems can be rewritten as the solution of the following three minimization problems:

$$\|p_g(t) - f(\hat{p}_0(t),h_g(t),c_s(t))\|^2 < \epsilon, \quad (8)$$

$$\|p_g(t) - f(p_0(t),\hat{h}_g(t),c_s(t))\|^2 < \epsilon, \quad (9)$$

$$\|p_g(t) - f(p_0(t),h_g(t),\hat{c}_s(t))\|^2 < \epsilon, \quad (10)$$

where ϵ denotes the tolerance of the convergence process. The minimization problem is solved with the *Newton algorithm*. The inversion process of the steady Poiseuille model can be repeated for each time instant independently or applied to a whole signal in order to obtain the searched quantity at all time instants. The position of the separation point $x=s$ and, consequently, the constriction height at separation h_s depends on the minimum constriction height h_g and the separation coefficient c_s due to the separation criterion $h_s = c_s h_g$. Therefore, the position of the separation point varies during the convergence process of minimization problems (9) and (10). The moving separation point introduces numerical discontinuities in the minimization function when a spatial discretization of the geometry is used. This is avoided by approximating the integral in Eq. (2) with a *Gauss–Chebychev* quadrature (Kincaid and Cheney, 1996)

c. Inverse unsteady Bernoulli model. The three inversion problems for the unsteady Bernoulli model (BU-d) defined by the sum of the pressure terms (1) and (3) are solved following the same approach as for the PS-d model, i.e., using numerical iterative methods. As for the steady Poiseuille model, the spatial discretization of the geometry is again avoided by approximating the integral in Eq. (3) with a Gauss–Chebychev quadrature. Contrary to the steady models, the inversion process is applied to an entire time range in order to reduce the error propagation on the inverted values, since due to Eq. (3), the predictions at instant $t=i$ are dependent on the predictions at previous instants $t<i$.

d. Inverse unsteady Poiseuille model. The strategy used for the inversion of the unsteady Poiseuille model (PU-d) is similar to the approach outlined for the inversion of the unsteady Bernoulli model.

III. THEORETICAL STUDY AND DISCUSSION

The accuracy of the inverse models with respect to theoretical simulations of the corresponding direct models is discussed in this section. The outcome of the direct models is used as the input of the inverse models in order to reestimate the original input variables of the direct models. The influence of the pressure terms, which are expressed in Eqs. (1)–(3), on the simulated results is discussed. The glottal geometry is approximated by the varying channel height $h(x)$ between two half circles with 1 cm radius, depicted in Fig. 5(d) and the upstream channel height of $h_0=23.6$ mm. The importance of the flow model parameter c_s related to flow separation in the diverging downstream part of the constriction can be assessed.

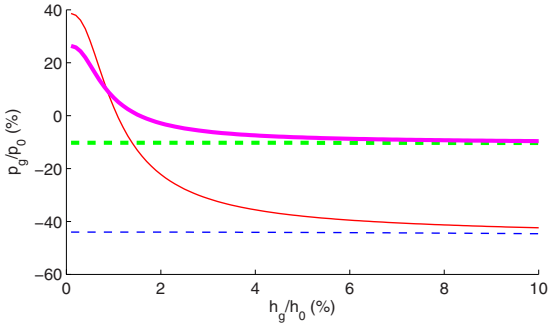

FIG. 2. (Color online) Theoretical simulations for steady flow conditions with a round constriction and upstream pressure $p_0=100$ Pa. Ratio between the pressure at the minimum constriction height and the upstream pressure p_g/p_0 as function of the ratio between the minimum constriction height and the upstream height h_g/h_0 for BS-d model with $c_s=1.05$ (thick dashed line) and $c_s=1.2$ (thin dashed line) and for PS-d model with $c_s=1.05$ (thick solid line) and $c_s=1.2$ (thin solid line).

A. Steady flow conditions

Steady flow conditions allow one to study the importance of the Poiseuille pressure term (2) on the model predictions compared to the Bernoulli pressure term (1).

1. Steady Bernoulli model

The normalized pressure at the minimum constriction height, p_g/p_0, predicted by the direct steady Bernoulli model (BS-d) is quantitatively illustrated in Fig. 2. For a fixed upstream pressure $p_0=100$ Pa, the minimum constriction height is decreased from 10% down to 0% of the upstream channel height and two separation coefficients, $c_s=1.05$ and $c_s=1.2$, are considered. In accordance with Eq. (7) the pressure drop p_g obtained from the steady Bernoulli model is fully determined by the choice of the separation coefficient c_s. Regardless of the minimum height h_g, the pressure ratio p_g/p_0 yields respectively -10% and -44% for c_s set to 1.05 and 1.2. This way, the separation coefficient c_s determines the position of flow separation through the *ad hoc* relation $h_s=c_s h_g$, the magnitude of the pressure drop as well as the spatial range in which the glottal flow exerts pressure forces on the surrounding walls. In addition, increasing c_s increases the estimated volume flow rate Φ. Since the three inverse models (BS-inv1, BS-inv2, and BS-inv3) outlined in Sec. II C 2 a are analytically derived from the direct model (BS-d), the estimated inverse model outcomes $\hat{p}_0$, $\hat{h}_g$, or $\hat{c}_s$ match the direct model input parameters exactly.

2. Steady Poiseuille model

The addition of the Poiseuille term (2) in the flow model has a major effect on the pressure predictions for small minimum apertures (Ruty *et al.*, 2007), as illustrated in Fig. 2. The discrepancy between BS-d and PS-d predictions of $\hat{p}_g$ increases as the ratio h_g/h_0 decreases. Moreover, the contribution of the Poiseuille term results in positive $\hat{p}_g$ estimates for $h_g/h_0 \leqslant 2\%$. The separation coefficient c_s is again a significant parameter for PS-d since increasing c_s increases the magnitude of the viscous contribution. In general, viscous effects should not be neglected for small apertures, i.e., for $h_g/h_0 < 10\%$ ratios. By accounting for viscous effects, the flow circulation is assumed to be more difficult so that the volume flow rate predicted by PS-d is slightly below the BS-d estimation. Moreover, even if the volume flow rates predicted by both models are very close, their relative difference increases as the constriction height decreases. Inversion of PS-d is obtained numerically, following the minimization procedure outlined in Sec. II C 2 b. The inverse model accuracy and the required number of iterations rely on the convergence parameter ϵ in Eqs. (8)–(10). The choice of ϵ relies on a trade-off between the precision of the inverse model results and the required computation time. By setting $\epsilon=10^{-8}$ in PS-inv1, PS-inv2, and PS-inv3, the error introduced by the inversion process becomes negligible and the convergence can be obtained within 20 iterations regardless of the searched variable.

B. Unsteady flow conditions

Variations in time of the upstream pressure $p_0(t)$ and/or the minimum constriction height $h_g(t)$ can affect the flow characteristics. Introducing time dependency in the direct and inverse flow model descriptions allows one to account for flow effects due to unsteadiness. As mentioned in Secs. II A and II B 1, the glottal flow is assumed to be quasisteady during normal phonation since typically $\mathrm{Sr}=10^{-2}$ holds (Zhang *et al.*, 2002). During singing, abnormal phonation or in case of vocal fold pathologies, the glottal flow might be characterized by a greater Strouhal number. This can result from an increase in the fundamental frequency f or the vocal folds length L so that unsteadiness effects can become important. Moreover, unsteadiness effects are known to be important during glottal closure (Deverge *et al.*, 2003). In Secs. III B 1 and III B 2, the unsteady Bernoulli and Poiseuille models are considered. The reported validation passes the limits of the physical values encountered during *in vivo* phonation in order to fully validate the inversion process. Due to unsteadiness, the occurrence of flow separation and jet formation is known to depend on the Reynolds number and the Strouhal number (Sobey, 1983). Classical phonation models assume a constant flow separation coefficient. In the following, the separation coefficient $c_s(t)$ is assumed to be able to vary in time.

1. Unsteady Bernoulli

The discrepancies between $\hat{p}_g(t)$ and $\hat{\Phi}(t)$ predictions obtained with BS-d and BU-d are illustrated in Fig. 3. The simulations are obtained for the round constriction shape depicted in Fig. 5(d). The input signals $p_0(t)$, $h_g(t)$, and $c_s(t)$ are varying in time with frequencies of 300, 500, and 100 Hz, respectively. These frequencies are chosen arbitrarily different in order that effects related to each parameter can be individually identified in the output waveforms. The input signals cannot be compared to those observed *in vivo*. The variation of $h_g(t)$ corresponds to $\mathrm{Sr}\approx 0.3$ so that unsteadiness has a visible influence on the models predictions. Comparing $\hat{p}_g(t)$ signals, it can be observed that the BS-d estimation is fully determined by $c_s(t)$ contrary to the BU-d estimation which presents amplitude variations due to the dependency on $h_g(t)$ expressed in Eq. (3). Thus, BU-d predicts a greater

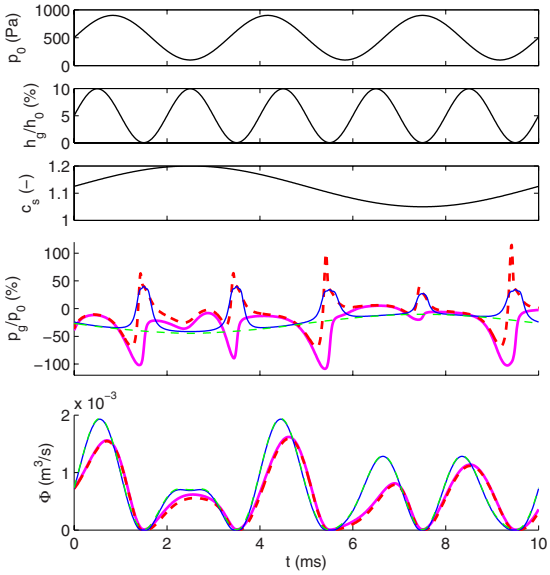

FIG. 3. (Color online) Theoretical simulations for unsteady flow conditions with a round constriction. (Three top figures) Input signals of the upstream pressure p_0, the ratio between the minimum constriction height and the upstream height h_g/h_0 and the separation coefficient c_s. (Middle) Simulated signals of the ratio between the pressure at the minimum constriction height and the upstream pressure p_g/p_0. (Bottom) Simulated signals of volume flow rate Φ. Frequency of h_g vibration is 500 Hz corresponding to Sr ≈ 0.3. Output signals are simulated by BS-d (thin dashed line), PS-d (thin solid line), BU-d (thick solid line) and PU-d (thick dashed line).

pressure drop at the minimum constriction height during the constriction closure. On the contrary, the pressure drop predicted by BU-d when the constriction is more widely open is less important than the one predicted by BS-d. The addition of Eq. (3) in the direct modeling introduces magnitude and phase differences between the volume flow rate signals generated by BS-d and BU-d, as shown in Fig. 3. Inversion of BU-d is obtained numerically as outlined in Sec. II C 2 c. The approximations introduced by the convergence process in the estimated signals $\hat{p}_0(t)$, $\hat{h}_g(t)$, and $\hat{c}_s(t)$ can be considered as negligible, as discussed in Sec. III A 2. However, despite the application of the inversion process to an entire signal, the error propagation in time can lead to inaccurate estimations at the end of the signal.

2. Unsteady Poiseuille

In PU-d, two additional pressure terms are in competition for the prediction of the flow characteristics. In Fig. 3, it can be seen that the $\hat{p}_g(t)$ signals generated by BU-d and PU-d are similar when the constriction is open. However, when the constriction is closing, viscous effects become predominant so that the $\hat{p}_g(t)$ predicted by PU-d is closer to the prediction of PS-d. Besides, viscous effects seems to be emphasized by the unsteady flow conditions since the maximum pressure peaks observed for PU-d at the constriction closure instant are higher than those observed for PS-d whereas BU-d predicts negative pressures. Concerning the volume flow rate predictions, the Poiseuille pressure term (2) has a minor influence. Thus, in Fig. 3, the $\hat{\Phi}(t)$ signals predicted by BS-d and PS-d are quasisuperposed. As noticed in Sec. III B 1, the addition of Eq. (3) in the direct modeling introduces magnitude and phase differences between the $\hat{\Phi}(t)$ signals predicted by steady and unsteady models so that the BU-d and PU-d predictions are also quasisuperposed. The considerations about the inversion of BU-d made in Sec. III B 1 hold for the inversion of PU-d.

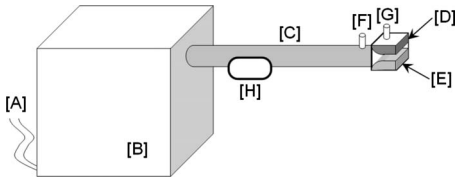

FIG. 4. Schematic representation of the experimental setup: [A] air supply, [B] pressure tank, [C] upstream pipe, [D,E] rigid vocal fold replica, [F,G] pressure taps, and [H] volume flow rate meter.

IV. *IN VITRO* VALIDATION AND DISCUSSION

The high accuracy of the inverse flow models, described in Sec. II C with respect to data obtained by simulations with the corresponding direct flow models, is pointed out in the previous Sec. III. This section assesses the validation of the inverse flow models against *in vitro* experimental data. The validity of the inverse flow models for real world flow data is likely to depend on the accuracy of the direct flow models. Therefore, the *in vitro* validation of the inverse steady and unsteady flow models, presented in, respectively, Secs. IV A and IV B, is inspired on the *in vitro* validation of flow models with glottal constriction rigid replicas reported in *a.o.* Deverge *et al.* (2003); Hofmans *et al.* (2003); Pelorson *et al.* (1994); Ruty *et al.* (2007); Van Hirtum *et al.* (2007); Vilain *et al.* (2004).

A. Steady flow conditions

The inverse model validation for steady flow conditions aims to quantify the influence of taking into account the viscosity and of the choice of the separation coefficient on the inverse model performance.

1. Setup for steady flow measurements

The experimental setup is schematically depicted in Fig. 4. Steady flow is provided by a valve controlled air supply [A] connected to a pressure tank of 0.75 m^3 [B] enabling to impose an airflow through the rigid vocal fold replica [D,E]. An upstream pipe [C] of 95 cm is used to prevent from turbulent flow at the replica position. Pressure transducers (Endevco 8507C or Kulite XCS-093) are positioned in pressure taps upstream of the replica [F] and at the minimum constriction height of the constriction [G] allowing to measure the upstream pressure p_0 and the pressure at the minimum constriction height p_g. The volume flow rate Φ is measured (TSI 4000) upstream of the constriction [H]. The *in vitro* constriction is formed by two vocal fold metal replicas in a fixed position. The minimum constriction height h_g between the two rigid vocal folds can be changed by means of two adjustment screws. Different minimum constriction heights are studied: h_g=0.2 mm, h_g=0.5 mm, and h_g =1.0 mm. Two different constriction shapes depicted in Fig. 5 are considered, (a) uniform (with a rounded entrance) and

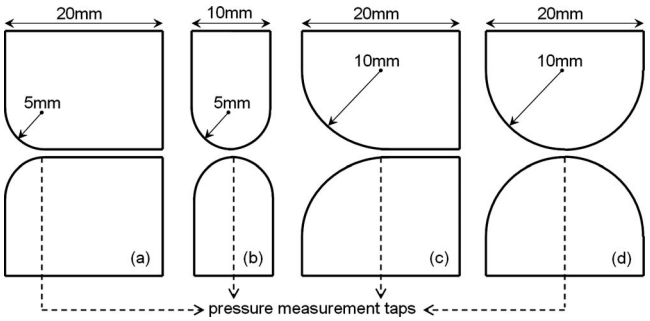

FIG. 5. Geometries of the rigid vocal fold replicas. Uniform (a) and round (b) constriction for steady flow measurements. Uniform (c) and round (d) constriction for unsteady flow measurements.

(b) round, in order to favor either the study of viscous wall effects or flow separation.

2. Uniform Constriction

A uniform channel is particularly interesting to evaluate the flow modeling with respect to viscous wall effects without interference of the flow separation position. For a uniform constriction, flow separation always occurs at the constriction end so that $h_g=h_s$. This implies that $c_s=1$ so that c_s is no further considered in this section. Therefore, two inversion problems are maintained in order to retrieve respectively the upstream pressure $\hat{p}_0$ (-inv1) and the minimum constriction height $\hat{h}_g$ (-inv2). Measurements of p_0, p_g, and Φ are presented in Fig. 6. The upstream pressure p_0 covers the

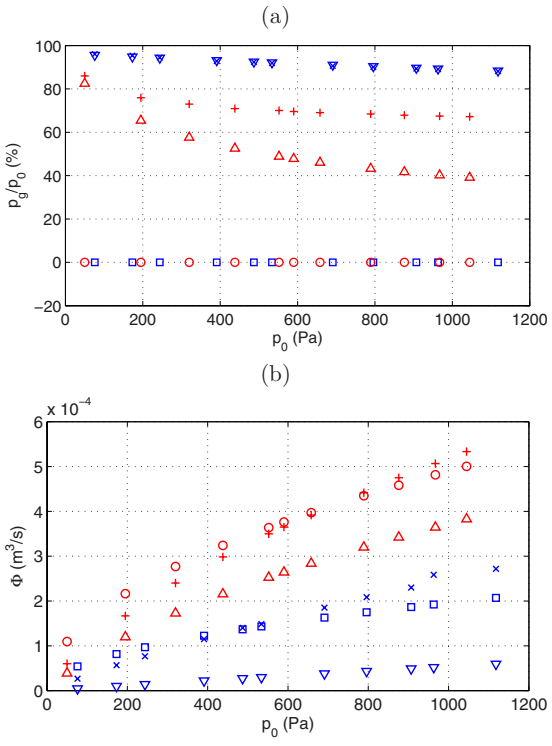

FIG. 6. (Color online) (a) Ratio between pressure at the minimum constriction height and upstream pressure p_g/p_0 and (b) volume flow rate Φ as function of the upstream pressure p_0 measured for steady flow conditions with the uniform constriction, for the minimum constriction heights h_g =0.2 mm (×) and h_g=0.5 mm (+). The corresponding predictions of the *Bernoulli* (□, ○) and Poiseuille (▽, △) models are shown.

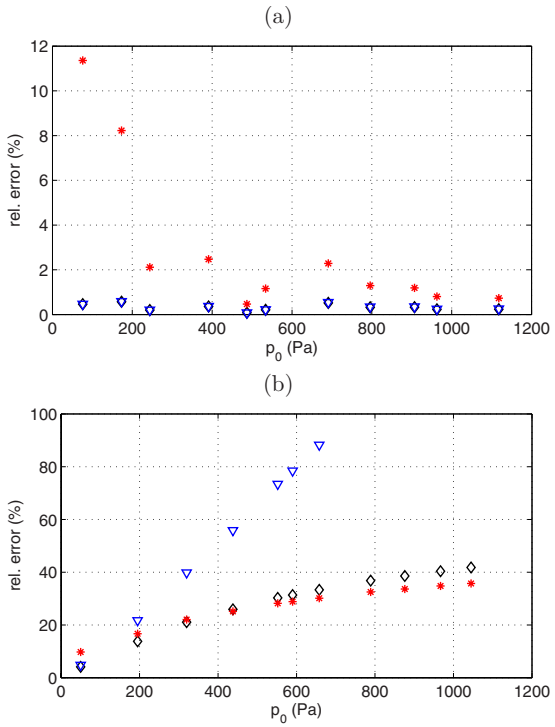

FIG. 7. (Color online) Relative errors of the steady Poiseuille models predictions compared to the steady experimental measurements performed with the uniform constriction for (a) h_g=0.2 mm and (b) h_g=0.5 mm: pressure at the minimum constriction p_g (PS-d, ◇), upstream pressure p_0 (PS-inv1, ▽) and minimum constriction height h_g (PS-inv2, ∗).

range of interest from 100 up to 1000 Pa and h_g is set to 0.2 and 0.5 mm. Predictions of $\hat{p}_g$ and $\hat{\Phi}$ given by BS-d and PS-d are shown. Following Eq. (7), BS-d predicts $\hat{p}_g$ to be equal to the downstream pressure, i.e., $\hat{p}_g=p_s=0$, regardless of p_0 and h_g. Therefore, BS-inv1 and BS-inv2 are not applicable and are not further illustrated in this section. It can be observed from Fig. 6(a) that PS-d predicts the measured pressure data with 1% for h_g=0.2 mm. In this case, the gap between the vocal fold replicas is very narrow compared to the upstream height ($h_g/h_0 \leqslant 10\%$), which indicates that viscous effects are predominant in the pressure determination and allow one to explain the very accurate pressure predictions of PS-d. For h_g=0.5 mm, the prediction error increases from 10% to 40% for p_0 increasing from 100 to 1000 Pa. In this case, viscous effects are less important and their approximation by the Poiseuille pressure term (2) does not allow to obtain accurate pressure predictions compared to *in vitro* measurements. Concerning the volume flow rate, Fig. 6(b) shows that BS-d predicts the measured data more accurately than PS-d for h_g=0.2 mm and h_g=0.5 mm. For the inverse modeling, Fig. 7 presents the relative errors between the measurements and the predictions made by PS-d, PS-inv1, and PS-inv2. This figure illustrates, in a quantitative way, the link between the predictions errors of the direct and inverse models. For h_g=0.2 mm [Fig. 7(a)], PS-inv1 predicts the measured upstream pressure p_0 within 1%, which is similar to the PS-d predictions accuracy. On the other hand, the inverse estimation of h_g with PS-inv2 appears to be more sensitive to the error made with PS-d since an error of 1% for $\hat{p}_g$ can yield up to an error of 10% for $\hat{h}_g$, in particular, for low

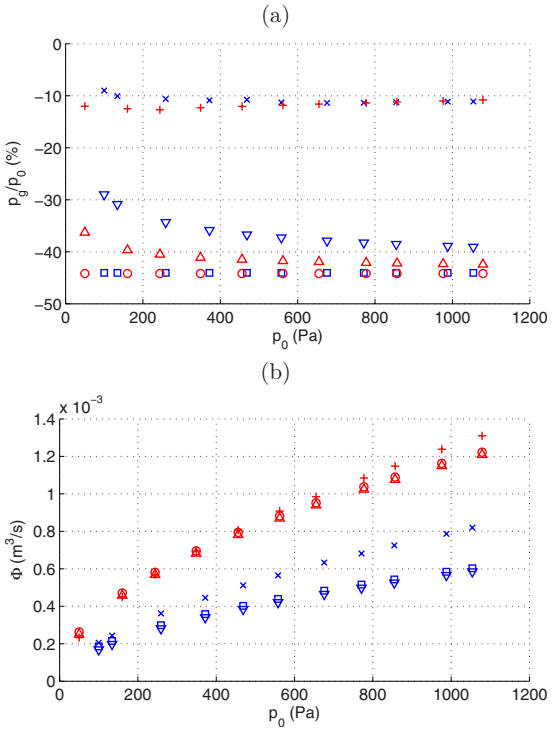

FIG. 8. (Color online) (a) Ratio between pressure at the minimum constriction height and upstream pressure p_g/p_0 and (b) volume flow rate Φ as function of the upstream pressure p_0 measured for steady flow conditions with the round constriction, for the minimum constriction heights h_g =0.5 mm (×) and h_g=1.0 mm (+). The corresponding predictions of the Bernoulli (□, ○) and Poiseuille (▽, △) models using c_s=1.2 are shown.

Reynolds numbers corresponding to low upstream pressures. For h_g=0.5 mm [Fig. 7(b)], it can be noticed that the inverse model error rates are proportional to the error rate of the direct model. In this case, the inverted upstream pressure $\hat{p}_0$ is largely overestimated and the corresponding error reaches more than 100%. The error rate of the PS-inv2 predictions is similar to the one observed for PS-d predictions. Thus, steady Poiseuille models predictions become less accurate as the experimental minimum constriction height and the upstream pressure increase.

3. Round constriction

The influence of the flow separation coefficient can be studied with a round constriction geometry since flow separation occurs in the diverging downstream part. In the quasi-one-dimensional models under study, the flow separation position is determined by the choice of the flow separation coefficient c_s. In order to limit the influence of viscous wall effects, the minimum constriction heights of h_g=0.5 mm and h_g=1.0 mm are experimentally assessed. The BS-d and PS-d predictions of the pressure $\hat{p}_g$ and the volume flow rate $\hat{\Phi}$ computed with c_s=1.2 are presented in Fig. 8 as well as the *in vitro* measurements. The value c_s=1.2 is commonly found in literature. Therefore, $h_s=c_s h_g$ yields 0.6 and 1.2 mm, respectively. As for the uniform constriction, the PS-d predictions are closer to the experimental pressure data, as shown in Fig. 8(a), even if both direct models overestimate (by a factor of 3–4) the pressure drop at the minimum constriction height. Likewise, the volume flow rate predictions given by

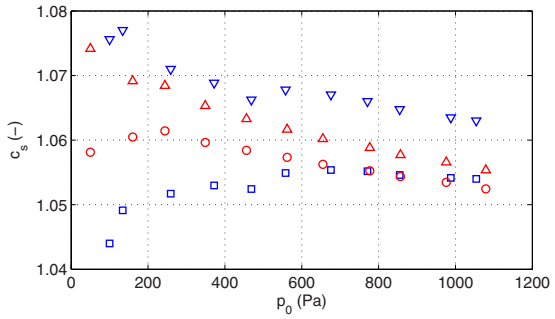

FIG. 9. (Color online) Estimation of the separation coefficient c_s from experimental measurements performed with the round constriction for h_g =0.5 mm and h_g=1.0 mm with the inverse Bernoulli (□, ○) and Poiseuille (▽, △) models.

BS-d are closer to the experimental measurements than the predictions given by PS-d. However, the difference between the BS-d and PS-d predictions decreases with increasing h_g. Regarding the pressure determination, the model's accuracy appears to depend mainly on the choice of c_s since the measured pressure ratios p_g/p_0 are about −10% and corresponds to a smaller separation coefficient. This is illustrated in Fig. 9, where Bs-inv3 and PS-inv3 are applied in order to estimate the separation coefficient $\hat{c}_s$ which best fits the experimental data for both assessed minimum apertures. The separation coefficient estimations are clearly smaller than 1.2 and moreover are found to vary as function of the Reynolds number (Sobey, 1983). Therefore, from Fig. 9, the mean value c_s=1.06 seems to be more adapted to the experimental conditions. Figure 10 shows the predictions $\hat{p}_g$ (a) and $\hat{\Phi}$ (b) given by BS-d and PS-d using this value of c_s. Thus, the model's accuracy is improved for the estimation of p_g, but the change in c_s increases the discrepancy between the estimated and measured flow rates.

B. Unsteady flow conditions

The unsteady Bernoulli and Poiseuille models include the unsteadiness pressure term (3). In this section, the inverse model's validity is tested against *in vitro* measurements performed on the setup outlined in Sec. IV B 1 for unsteady flow conditions. The results obtained for respectively uniform and round replicas are discussed in Secs. IV B 2 and IV B 3 illustrating both the steady and unsteady model's predictions.

1. Setup for unsteady flow measurements

The experimental setup used to perform steady flow measurements is maintained to perform unsteady flow measurements. The setup is schematically depicted in Fig. 4 and is described in Sec. IV A 1. The unsteady flow conditions are obtained thanks to a moving rigid constriction replica previously used and described in Deverge *et al.* (2003); Vilain *et al.* (2004). Flow variations are generated by the driven movement of one of the rigid vocal fold replicas ([E] in Fig. 4). The frequencies f under consideration are included between 3 and 30 Hz, corresponding to Strouhal numbers in the range of 10^{-3}–10^{-2}. The resulting time varying constriction height $h_g(t)$ is measured by means of an optical sensor

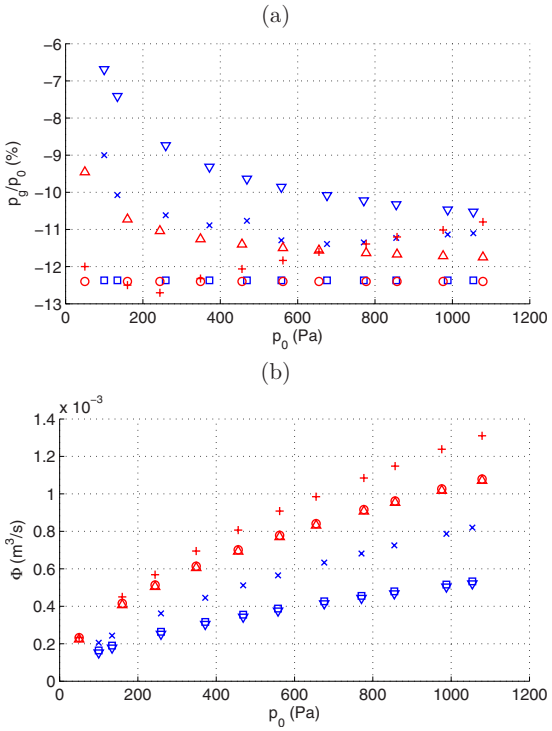

FIG. 10. (Color online) (a) Ratio between pressure at the minimum constriction height and upstream pressure p_g/p_0 and (b) volume flow rate Φ as function of the upstream pressure p_0 measured for steady flow conditions with the round constriction, for the minimum constriction heights h_g =0.5 mm (×) and h_g=1.0 mm (+). The corresponding predictions of the Bernoulli (□, ○) and Poiseuille (▽, △) models using c_s=1.06 are shown.

(OPB700). Two different constriction shapes depicted in Fig. 5 are considered: (c) uniform (with a rounded entrance) and (d) round.

2. Uniform constriction

As for steady flow conditions, a uniform constriction is assessed in order to rule out the influence of the choice of the separation coefficient on the model outcome since in this case, c_s=1. Therefore, the direct and inverse Bernoulli and Poiseuille models are validated with respect to unsteadiness. Three periods of measured and modeled signals obtained for a driving frequency of 25 Hz are shown in Fig. 11. It can be observed that direct Bernoulli models, BS-d and BU-d, are unable to predict the measured $p_g(t)$ so that the corresponding inverse models are not considered in the following. Besides, for the Strouhal number under consideration, Sr $\approx 10^{-2}$, unsteadiness has a minor impact on the pressure determination so that the $\hat{p}_g(t)$ signals given by steady and unsteady models appear quasisuperposed in Fig. 11. Thus, both direct Poiseuille models, PS-d and PU-d, predict the experimental pressure $p_g(t)$ within 20%. These two models provide a good approximation of the timing and the amplitude of the $p_g(t)$ signal. Therefore, PS-inv2 and PU-inv2 also give accurate results estimating the imposed minimum constriction height $h_g(t)$ with a mean error less than 15%. On the contrary, it can be observed that PS-inv1 and PU-inv1 are not able to estimate correctly the input upstream pressure $p_0(t)$. Indeed, the maximum error can reach 100% even if the mean error is less than 40%.

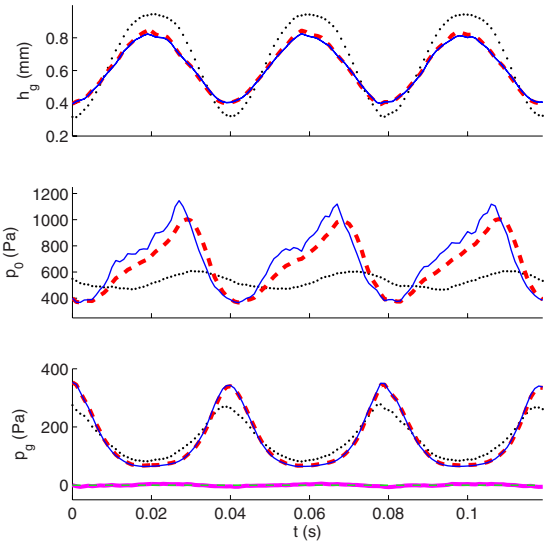

FIG. 11. (Color online) Measurements (●) and models predictions for the uniform vocal folds vibrating at 25 Hz ($S \approx 10^{-2}$): (top) minimum constriction height h_g, (middle) upstream pressure p_0 and (bottom) pressure at the minimum constriction height p_g. Predictions are given by the steady Bernoulli (thin dashed line), steady Poiseuille (thin solid line), unsteady Bernoulli (thick solid line) and unsteady Poiseuille (thick dashed line) models.

3. Round constriction

Figure 12 shows three periods of the measured and predicted signals for a round constriction vibrating at 25 Hz. The model signals presented in this figure are computed using c_s=1.2. As for the uniform constriction, direct flow modeling is significantly improved when viscous effects are taken into account. This can be observed from both the timing and the order of magnitude of $\hat{p}_g(t)$ predicted by PS-d and PU-d. Nevertheless, the overall accuracy of the direct Poiseuille models is low since the pressure drop is largely

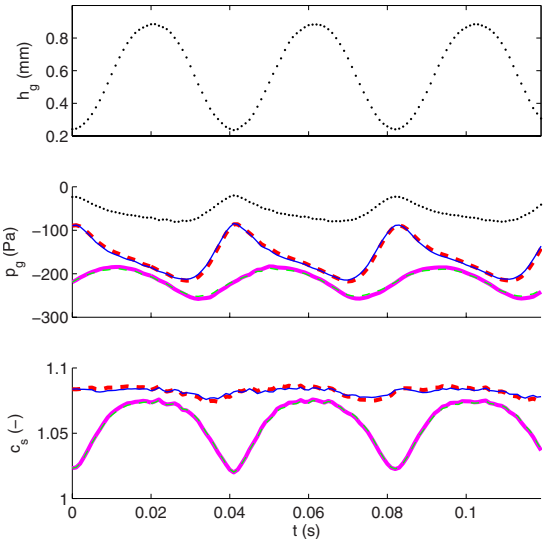

FIG. 12. (Color online) Measurements (●) and models predictions for the round vocal folds vibrating at 25 Hz ($S \approx 10^{-2}$): (top) minimum constriction height h_g, (middle) pressure at the minimum constriction height p_g (computed with c_s=1.2) and (bottom) inverted separation coefficient c_s. Predictions are given by the steady Bernoulli (thin dashed line), steady Poiseuille (thin solid line), unsteady Bernoulli (thick solid line) and unsteady Poiseuille (thick dashed line) models.

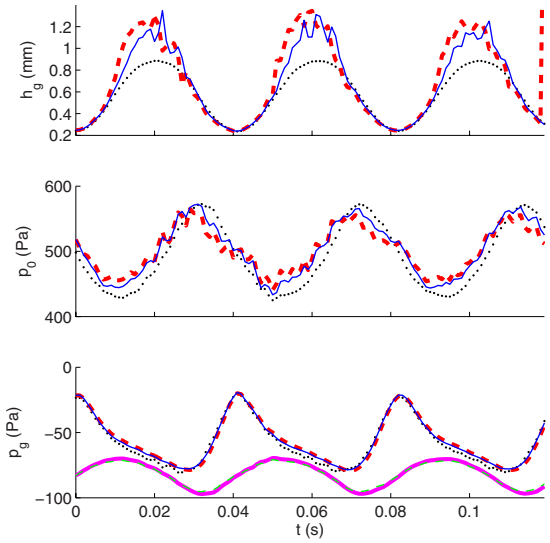

FIG. 13. (Color online) Measurements (●) and models predictions for the round vocal folds vibrating at 25 Hz (Sr≈10^{-2}): (top) minimum constriction height h_g, (middle) upstream pressure p_0 and (bottom) pressure at the minimum constriction height p_g. Predictions are computed with $c_s=1.08$ and given by the steady Bernoulli (thin dashed line), steady Poiseuille (thin solid line), unsteady Bernoulli (thick solid line) and unsteady Poiseuille (thick dashed line) models.

overestimated, resulting in a mean error exceeding 100%. Previously, the severe impact of the choice of the separation coefficent c_s on the predictions accuracy is extensively shown. Therefore, the separation coefficient is estimated from the measured data with the inverse models (-inv3). The estimated $\hat{c}_s$ is illustrated at the bottom of Fig. 12. PS-inv3 and PU-inv3 yield $c_s \approx 1.08$, whereas for BS-inv3 and BU-inv3, $\hat{c}_s$ varies between 1.02 and 1.07. Due to the poor qualitative accuracy of BS-d and BU-d and the inconsistent values of $\hat{c}_s$ given by BS-inv3 and BU-inv3, the value of $c_s=1.08$ obtained from PS-inv3 and PU-inv3 is used to re-estimate the direct and inverse models. The results are presented in Fig. 13 and show that the accuracy of the four direct models is largely improved. Since BS-d and BU-d are still unable to qualitatively predict $p_g(t)$, only the inverse Poiseuille models are considered to assess $\hat{p}_0(t)$ and $\hat{h}_g(t)$. As the PS-d and PU-d signals are very accurate predicting the measured $p_g(t)$ signal within 5%, the mean error of the PS-inv1 and PU-inv1 predictions is about 5% when c_s is set to 1.08. In this case, the mean error noticed for PS-inv2 and PU-inv2 is about 30%. This increased mean error is indeed due to a severe overestimation (greater than 50%) of the minimum constriction height when this one is large. The error amplification relative to direct Poiseuille models occurs when the viscosity related correction is the least effective, which shows the inaccuracy of the inviscid Bernoulli modeling. As for the uniform constriction, the steady model predictions match the unsteady model predictions to a fair extent in accordance with the low Strouhal number under consideration, Sr $\approx 10^{-2}$.

V. CONCLUSION

Inverse models derived from quasi-one-dimensional flow models commonly applied in simplified physical phonation models are formulated in order to retrieve the main physical variable and model parameters, i.e., the upstream pressure, the minimum constriction height, or the flow separation coefficient. The accuracy of the inverse models is validated firstly against theoretical simulations obtained with the corresponding direct models and secondly against *in vitro* experimental data. The proposed inverse models allow to retrieve quasiexactly the original direct model input with a minimum of computational effort. Moreover, the severe influence of flow separation, viscosity, and unsteadiness due to wall movement on the model predictions is pointed out for, respectively, a divergent round constriction shape, small apertures, and high Strouhal numbers. *In vitro* experimental validation in steady and unsteady flow conditions is achieved on rigid vocal folds replicas with uniform and round constriction shapes in order to study the impact of viscosity and flow separation on the inverse model performance. It appears that both viscosity and the flow separation position determine the relevance of the inverse quasi-one-dimensional models. A mean prediction accuracy of 20% for the searched physical variables can be achieved for a divergent round constriction shape when the flow modeling includes a viscosity related correction and uses a suitable separation coefficient. Remark that the necessity of a corrective term related to viscosity outlines the limitations of the one-dimensional inviscid Bernoulli model. Moreover, the prediction errors increase when the contribution of the viscosity related term to the pressure determination is less important. The performance of the inverse models is seen to reflect the accuracy of the direct models. Therefore, it seems interesting, on the one hand, to include the sensitivity to the input variables errors in the minimization problem and, on the other hand, to use more advanced flow models in order to validate the value of the separation coefficient. Indeed, this parameter is often chosen as a constant but this study confirms that it depends on the Reynolds number so that it should be adapted in accordance with the aimed range of flow conditions relvant to phonation.

ACKNOWLEDGMENTS

This work has been supported by a Ph.D. grant from the French Ministry of Education and Research. The authors wish to thank A. Hirschberg, Technical University of Eindhoven, The Netherlands, for kindly providing the moving rigid vocal fold replicas, D. Blanc and D. Rey, Département Automatique, GIPSA-Laboratory, France, for their help in building the experimental setup, and the anonymous reviewers for their helpful comments.

Alipour, F., and Scherer, R. (**2004**). "Flow separation in a computational oscillating vocal fold model," J. Acoust. Soc. Am. **116**, 1710–1719.
Alipour, F., and Scherer, R. (**2006**). "Characterizing glottal jet turbulence," J. Acoust. Soc. Am. **119**, 1063–1073.
Alku, P., Vilkman, E., and Laukkanen, A. (**1998**). "Estimation of amplitude features of the glottal flow by inverse filtering speech pressure signals," Speech Commun. **24**, 123–132.
Blevins, R. (**1992**). *Applied Fluid Dynamics Handbook* (Krieger, Melbourne, FL).
Cranen, B., and Boves, L. (**1988**). "On the measurement of glottal flow," J. Acoust. Soc. Am. **84**, 888–900.
Deverge, M., Pelorson, X., Vilain, C., Lagree, P., Chentouf, F., Willems, J.,

and Hirschberg, A. (**2003**). "Influence of collision on the flow through in-vitro rigid models of the vocal folds," J. Acoust. Soc. Am. **114**, 1–9.
Drioli, C. (**2005**). "A flow waveform-matched low-dimensional glottal model based on physical knowledge," J. Acoust. Soc. Am. **117**, 3184–3195.
Fant, G. (**1960**). *The Acoustic Theory of Speech Production* (Mouton de Gruyter, Berlin).
Frohlich, M., Michaelis, D., and Strube, H. (**2001**). "SIM-simultaneous inverse filtering and matching of a glottal flow model for acoustic speech signals," J. Acoust. Soc. Am. **110**, 479–488.
Grandchamp, X., Van Hirtum, A., and Pelorson, X. (**2007**). "Experimental validation of simplified free jet turbulence models applied to the vocal tract," *Proceedings of the 19th International Conference on Acoustics*, Madrid, Spain, p. 6.
Hertegard, S., and Gauffin, J. (**1995**). "Glottal area and vibratory patterns studied with simultaneous stroboscopy, flow glottography, and electroglottography," J. Speech Hear. Res. **38**, 85–100.
Hofmans, G., Groot, G., Ranucci, M., Graziani, G., and Hirschberg, A. (**2003**). "Unsteady flow through *in vitro* models of the glottis," J. Acoust. Soc. Am. **113**, 1658–1675.
Kelley, C. (**1995**). *Iterative Methods for Linear and Nonlinear Equations* (Society for Industrial and Applied Mathematics, Philadelphia, PA).
Kincaid, D., and Cheney, W. (**1996**). *Numerical Analysis* (Brooks-Cole, Pacific Grove, CA).
Kreiman, J., and Gerratt, B. (**2005**). "Perception of aperiodicity in pathological voice," J. Acoust. Soc. Am. **117**, 2201–2211.
Kundu, P. (**1990**). *Fluid Mechanics* (Academic, London).
Lagrée, P. (**2000**). "An inverse technique to deduce the elasticity of a large artery," Eur. Phys. J.: Appl. Phys. **9**, 153–163.
Lous, N., Hofmans, G., Veldhuis, N., and Hirschberg, A. (**1998**). "A symmetrical two-mass vocal-fold model coupled to vocal tract and trachea, with application to prosthesis design," Acta Acust. **84**, 1135–1150.
Lucero, J. (**1999**). "A theoretical study of the hystheresis phenomenon at vocal fold oscillation onset-offset," J. Acoust. Soc. Am. **105**, 423–431.
Mergell, P., Herzel, H., and Titze, I. (**2000**). "Irregular vocal-fold vibration, high-speed observation and modeling," J. Acoust. Soc. Am. **108**, 2996–3001.
Pelorson, X. (**2001**). "On the meaning and accuracy of the pressure-flow technique to determine constriction areas within the vocal tract," Speech Commun. **35**, 179–190.
Pelorson, X., Hirschberg, A., Van Hasselt, R., Wijnands, A., and Auregan, Y. (**1994**). "Theoretical and experimental study of quasisteady-flow separation within the glottis during phonation application to a modified two-mass model," J. Acoust. Soc. Am. **96**, 3416–3431.
Price, P. (**1989**). "Male and female voice source characteristics: inverse filtering results," Speech Commun. **8**, 261–277.
Qiu, Q., and Schutte, H. (**2006**). "A new generation videokymography for routine clinical vocal fold examination," Laryngoscope **116**, 1824–1828.
Rothenberg, M., and Zahorian, S. (**1977**). "Nonlinear inverse filtering techniques for estimating the glottal-area waveform," J. Acoust. Soc. Am. **61**, 1063–1071.
Ruty, N., Pelorson, X., Van Hirtum, A., Lopez, I., and Hirschberg, A. (**2007**). "An *in vitro* setup to test the relevance and the accuracy of low-order vocal folds models," J. Acoust. Soc. Am. **121**, 479–490.
Sciamarella, D., and d'Alessandro, C. (**2004**). "On the acoustic sensitivity of a symmetrical two-mass model of the vocal folds to the variation of control parameters," Acta Acust. **90**, 746–761.
Shadle, C. H., Barney, A., and Davies, P. O. A. L. (**1999**). "Fluid flow in a dynamic mechanical model of the vocal folds and tract. ii. implications for speech production studies," J. Acoust. Soc. Am. **105**, 456–466.
Sobey, I. (**1983**). "The occurrence of separation in oscillatory flow," J. Fluid Mech. **134**, 247–257.
Sundberg, J., Anderson, M., and Hultqvist, C. (**1999**). "Effects of subglottal pressure variation on professional baritone singers voice sources," J. Acoust. Soc. Am. **105**, 1965–1971.
Svec, J., Sram, F., and Schutte, H. (**2007**). "Videokymography in voice disorders: what to look for?," Ann. Otol. Rhinol. Laryngol. **116**, 172–180.
Van Hirtum, A., Cisonni, J., Ruty, N., Pelorson, X., Lopez, I., and van Uittert, F. (**2007**). "Experimental validation of some issues in lip and vocal fold physical models," Acta Acust. **93**, 314–323.
Vilain, C., Pelorson, X., Fraysse, C., Deverge, M., Hirschberg, A., and Willems, J. (**2004**). "Experimental validation of a quasi-steady theory for the flow through the glottis," J. Sound Vib. **276**, 475–490.
Wong, D., Ito, M., and Cox, N. (**1991**). "Observation of perturbations in a lumped-element model of the vocal folds with application to some pathological case," J. Acoust. Soc. Am. **89**, 383–394.
Wurzbacher, T., Schwarz, R., Dollinger, M., Hoppe, U., Eysholdt, U., and Lohscheller, J. (**2006**). "Model-based classification of nonstationary vocal fold vibrations," J. Acoust. Soc. Am. **120**, 1012–1027.
Zhang, Y., and Jiang, J. (**2004**). "Chaotic vibrations of a vocal fold model with a unilateral polyp," J. Acoust. Soc. Am. **115**, 1266–1269.
Zhang, Z., Mongeau, L., and Frankel, S. (**2002**). "Experimental verification of the quasisteady approximation for aerodynamic sound generation by pulsating jets in tubes," J. Acoust. Soc. Am. **112**, 1652–1663.